land

Article

Multi-Temporal Assessment of Remotely Sensed Autumn Grass Senescence across Climatic and Topographic Gradients

Lwando Royimani [1], Onisimo Mutanga [1,*], John Odindi [1] and Rob Slotow [2]

[1] Discipline of Geography, School of Agricultural, Earth and Environmental Sciences, University of KwaZulu-Natal, P/Bag X01, Scottsville, Pietermaritzburg 3209, South Africa
[2] School of Life Sciences, University of KwaZulu-Natal, Pietermaritzburg 3209, South Africa
* Correspondence: mutangao@ukzn.ac.za

Abstract: Climate and topography are influential variables in the autumn senescence of grassland ecosystems. For instance, extreme weather can lead to earlier or later senescence than normal, while higher altitudes often favor early grass senescence. However, to date, there is no comprehensive understanding of key remote-sensing-derived environmental variables that influence the occurrence of autumn grassland senescence, particularly in tropical and subtropical regions. Meanwhile, knowledge of the relationship between autumn grass senescence and environmental variables is required to aid the formulation of optimal rangeland management practices. Therefore, this study aimed to examine the spatial autocorrelations between remotely sensed autumn grass senescence vis-a-vis climatic and topographic variables in the subtropical grasslands. Sentinel 2′s Normalized Difference NIR/Rededge Normalized Difference Red-Edge (NDRE) and the Chlorophyll Red-Edge (Chlred-edge) indices were used as best proxies to explain the occurrence of autumn grassland senescence, while monthly (i.e., March to June) estimates of the remotely sensed autumn grass senescence were examined against their corresponding climatic and topographic factors using the Partial Least Square Regression (PLSR), the Multiple Linear Regression (MLR), the Classification and Regression Trees (CART), and the Random Forest Regression (RFR) models. The RFR model displayed a superior performance on both proxies (i.e., RMSEs of 0.017, 0.012, 0.056, and 0.013, as well as R^2s of 0.69, 0.71, 0.56, and 0.71 for the NDRE, with RMSEs and R^2s 0.023, 0.018, 0.014 and 0.056, as well as 0.59, 0.60, 0.69, and 0.72 for the Chlred-edge in March, April, May, and June, respectively). Next, the mean monthly values of the remotely sensed autumn grass senescence were separately tested for significance against the average monthly climatic (i.e., minimum (T_{min}) and maximum (T_{max}) air temperatures, rainfall, soil moisture, and solar radiation) and topographic (i.e., slope, aspect, and elevation) factors to define the environmental drivers of autumn grassland senescence. Overall, the results indicated that T_{max} (p = 0.000 and 0.005 for the NDRE and the Chlred-edge, respectively), T_{min} (p = 0.021 and 0.041 for the NDRE and the Chlred-edge, respectively), and the soil moisture (p = 0.031 and 0.040 for the NDRE and the Chlred-edge, respectively) were the most influential autumn grass senescence drivers. Overall, these results have shown the role of remote sensing techniques in assessing autumn grassland senescence along climatic and topographic gradients as well as in determining key environmental drivers of this senescence in the study area

Keywords: autumn senescence; grass; climate; remotely sensed; topographic factors

check for updates

Citation: Royimani, L.; Mutanga, O.; Odindi, J.; Slotow, R. Multi-Temporal Assessment of Remotely Sensed Autumn Grass Senescence across Climatic and Topographic Gradients. *Land* **2023**, *12*, 183. https://doi.org/10.3390/land12010183

Academic Editors: Michael Vrahnakis, Yannis (Ioannis) Kazoglou and Manuel Pulido Fernádez

Received: 28 November 2022
Revised: 29 December 2022
Accepted: 4 January 2023
Published: 6 January 2023

1. Introduction

Climate and topography are key drivers of plant phenology in terrestrial environments [1–7]. Their variability often influences the occurrence, rate, and duration of key phenological stages such as the autumn grassland ecosystem senescence. For instance, [6] noted a variation in the start of grass senescence in the low-lying Inner Mongolian grasslands than the higher Qinghai-Tibetian Plateau. However, the extent and significance of the overlaps between autumn grass senescence and environmental factors such as climate and topography have not been established, especially from a remote sensing point of view. Meanwhile, understanding the relationship between autumn grass senescence and environmental variables is vital, given that senescence markedly decreases photosynthetic activities and plant productivity [8], which, in turn, affects forage quality, production, and availability. Lwando Royimani et al. [9] also noted that senescence can either extend or reduce the floral species growing season with serious implications on forage productivity. In addition, studies [9–11] have noted the socioeconomic and ecological impact of grassland senescence including their regulatory role in the climate–biosphere interactions and potential contribution to land degradation [6]. Given the importance of rangelands and livestock farming for subsistence and commercial purposes, particularly in the developing world [2], knowledge on the implications of senescence on forage productivity in response to climatic and topographic gradients is increasingly becoming a need. This information is required to monitor the impact of autumn senescence on forage productivity [12], hence guiding planning and decision-making on, among others, grazing patterns and stock densities.

Useful assessment of the links between the occurrence of autumn grassland senescence and environmental variables at a landscape-scale requires repeated observations acquired at extensive spatial extents. However, the commonly used methods for assessing plant senescence, such as visual scoring, which monitors changes in leaf color and fall [11], do not effectively satisfy these requirements. Furthermore, these methods are generally not objective and suffer from the time lag effect [13]. Contrarily, remote sensing techniques offer repeated synoptic viewing of the Earth's surface [14–16], which may benefit the assessment of the spatial autocorrelations between grass senescence and environmental factors during the autumn season. Although many studies have examined plant senescence dynamics based on remote sensing techniques [13,17,18], few have focused on the interactions between autumn senescence and environmental parameters. For instance, [6] assessed the impact of temperature, insolation, and precipitation during the dormancy stage on China's temperate biomes using the Normalized Difference Vegetation Index (NDVI) derived over a 30-year period (1981–2011) from the Global Inventory Modeling and Mapping Studies (GIMMS). Their findings showed that temperature is a decisive factor to the end of the growing season. However, the study was generalized across biomes; hence, it did not offer an opportunity for a greater understanding of the autumn-senescence-environmental factors relationship in grassland environments, particularly in the subtropical regions.

In addressing this knowledge gap, the current study examines the spatial autocorrelations between remotely sensed autumn grass senescence and environmental parameters (i.e., climatic and topographic factors) in the subtropical sour-veld grasslands of the Midlands region, KwaZulu-Natal, South Africa, where autumn senescence is a key factor of forage productivity [9]. Such information is critical to ascertain the understanding of the dynamics around the occurrence of autumn grass senescence and to accurately determine grass wilting for improved planning and decision-making on grazing patterns and overall rangeland management. Specifically, a better understanding of the influence of environmental factors on autumn grass senescence will help improve the projection of the onset and duration of autumn grassland senescence, hence reliably determining the period of low- and poor-quality forage for grazing while minimizing the subsequent impact on livestock and wildlife. To achieve this aim, this study adopted two Sentinel-2-derived vegetation indices (i.e., the Normalized Difference NIR/Rededge Normalized Difference Red-Edge (NDRE) and the Chlorophyll Red-Edge (Chlred-edge)) that have been identified as the best proxies for explaining the occurrence of autumn grassland senescence within the study area [10]. Remotely sensed monthly (i.e., March to June) estimates of the autumn grass senescence were assessed for sensitivity against their corresponding climatic (i.e., minimum (T_{min}) and maximum (T_{max}) air temperatures, soil moisture, solar radiation, and rainfall) and topographic (i.e., slope, aspect, and elevation) factors using the Partial Least Squares Regression (PLSR), the Multiple Linear Regression (MLR), the Classification and Regression Trees (CART), and the Random Forest Regression (RFR) models. Next, monthly averages of the remotely sensed autumn grass senescence were tested against monthly mean values of the climatic and topographic variables using Pearson's product-moment correlation approach to understand possible environmental drivers of the autumn grass senescence. We hypothesized that the occurrence of autumn grass senescence in this area can be explained by the dynamics in the micro-climatic and topographic gradients.

2. Materials and Methods

2.1. The Study Site

The study area is situated in Vulindlela, KwaZulu-Natal, South Africa (Figure 1). The total size of the area is 112 km^2 and is characterized by rigid terrain with an elevation ranging between 1273 and 1412 m above sea level (m.a.s.l). The soils are generally loam with random rocky surfaces. Average annual rainfall is around 900 mm [19,20] with mean annual minimum and maximum air temperatures of 6 °C and 22 °C in winter and summer, respectively. Vegetation is mesic subtropical grass, dominated by the Ngongoni (*Aristida junciformis*) of the sour-veld, a mixture of non-native grass species and a random distribution of wattle and pine [10]. Sour-veld grasses are reported to lose their quality through senescence, thus significantly affecting their grazing importance [9]. In addition, grasses in the study area are subjected to regular and uncontrolled livestock grazing patterns, which may have serious implications on the forage. Moreover, irregular fire occurrences are common, especially during the winter season when the grasses are dry due to senescence, in turn affecting forage availability.

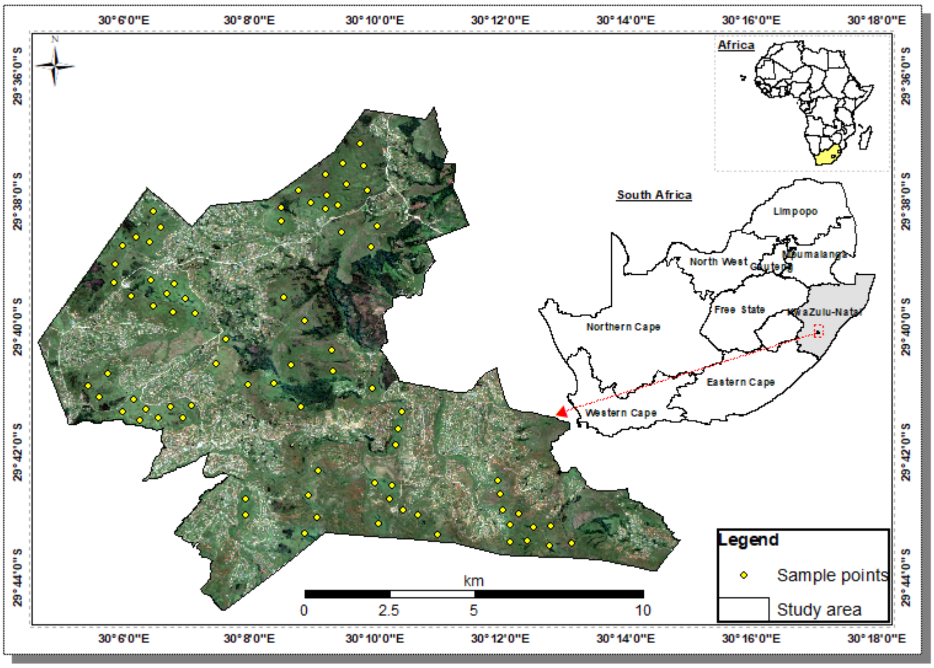

Figure 1. Location of the study area in Vulindlela, KwaZulu-Natal, South Africa and sampling sites.

2.2. Field Data Collection

A purposive sampling approach was used to establish 110 plots measuring about 10 m by 10 m and their center coordinates recorded. The plots were designed to provide a representation of the topography of the study site, particularly with regard to the elevation, aspect, and slope. For instance, some plots were created in low, middle, and high altitudinal areas while considering the effect of south-, east-, west-, and north-facing slopes. Equally, we considered the effect of the slope gradient whereby some plots were designed on steeper while others on gentle slopes. Soil moisture content readings were collected monthly within the plots using the ML3 ThetaProbe Soil Moisture Sensor between the 20 March and 30 June 2021. The ML3 ThetaProbe Soil Moisture Sensor measures soil moisture from the Earth's surface to the depth of 7 cm and the measurements are often expressed in percentage per volumetric water content (%/VWC) [21]. In this study, five measurements were randomly taken within each plot and averaged to obtain a value for the plot, and the points ultimately added up to 110 monthly values. Subsequently, we created four monthly point maps of the soil moisture with the corresponding coordinate points for the months of March, April, May, and June.

2.3. Remotely Sensed Autumn Grass Senescence

Two vegetation indices (i.e., the NDRE and the Chlred-edge), identified as the best proxies in explaining the occurrence of autumn grassland senescence in this area, were adopted [10]. These indices were derived from monthly Sentinel 2 images acquired using the Copernicus Open Access Hub data repository between the 29 March and 25 June 2021. Formulas for these indices are given in Equations (1) and (2). For detailed explanation on the establishment and validation of the named indices, readers are directed to [10]. The considered indices were derived on a monthly basis representing March, April, May, and June 2021. In total, eight vegetation index maps were generated, with four monthly indices generated using the NDRE and the Chlred-edge.

$$\mathrm{NRE} = \mathrm{NIR} - \mathrm{rededge}/\mathrm{NIR} + \mathrm{rededge} \tag{1}$$

where NIR is the Near-Infrared band and rededge is the red-edge (band).

$$\mathrm{Chlred\text{-}edge} = (\mathrm{R}_{0.705} - \mathrm{R}_{0.740})/(\mathrm{R}_{0.783} - \mathrm{R}_{0.740}) \tag{2}$$

where $R_{0.705}$ and $R_{0.783}$ correspond to the boundary wavebands while $R_{0.740}$ denotes the center waveband of the red-edge section.

2.4. Climatic and Topographic Variables

Daily rainfall and minimum (T_{min}) and maximum (T_{max}) air temperature data for the study area were acquired from the South African Weather Service (SAWS). The daily rainfall and temperature values were aggregated to obtain monthly records. However, these data were provided as point data for the city of Pietermaritzburg, hence being inadequate for analysis. Therefore, additional monthly T_{min} and T_{max} and rainfall data were downloaded from the KwaZulu-Natal Sugarcane Research Institute (KZN-SRI) website. Whereas the KZN-SRI has many weather stations distributed throughout the province of KwaZulu-Natal, we only used data from 22 stations that are surrounding the study site. The 22 weather stations are in a radius of 10 to 70 km from the central point of the study area across the eastern, northern, southern, and western directions. Next, we interpolated the combined KZN-SRI and SAWS data using the Inverse Difference Weighted (IDW) technique in ArcGIS 10.7 to generate a comprehensive T_{min} and T_{max} as well as rainfall data for the study site. Detailed descriptions of the topographic and climatic factors used are given in Table 1.

Table 1. Topographic plus climatic variables used in this study.

Variable	Units of Measurement	Source
	Topographic factors	
Aspect	Degrees North (°N)	ASTER DEM
Elevation	Miters (m)	ASTER DEM
Slope	Degrees (°)	ASTER DEM
	Climatic factor	
T_{min}	Degrees Celsius (°C)	SAWS, KZN-SRI
T_{max}	Degrees Celsius (°C)	SAWS, KZN-SRI
Rainfall	Millimeters (mm)	SAWS, KZN-SRI
Radiation	Watts Hours per square meter (Wh/m^2)	ASTER DEM

Note: ASTER = Advanced Spaceborne Thermal Emission and Reflection Radiometer, DEM = Digital Elevation Model.

Aspect, slope, elevation, and radiation were derived from a 30 m Digital Elevation Model (DEM) in ArcGIS. Specifically, aspect and slope were, respectively, calculated using the aspect and slope functions under the surface tools in Spatial Analysis Tools, ArcGIS 10.7 (Environmental Systems Research Institute (ESRI), Johannesburg, South Africa). Similarly, radiation was derived using the Area Solar Radiation extension found under surface tools of the Spatial Analysis Tools, ArcGIS 10.7 (Environmental Systems Research Institute (ESRI), Johannesburg, South Africa). Studies show that the application of modeled solar radiation from the DEM is a widely accepted practice in ecological remote sensing [2,22–24].

2.5. Data Processing and Statistical Analysis

To ensure compatibility and consistency in all the monthly maps generated (i.e., Sections 2.3 and 2.4), we applied the nearest-neighbor resampling approach in ArcGIS 10.7 based on the same resolution. We then overlaid all the monthly vegetation indices plus topographic and climatic maps with their respective monthly point maps to extract the corresponding monthly climatic, topographic, and remotely sensed autumn grass senescence information. Although the total number of the corresponding sampling points was 110, during data preparation, we discovered that 10 of those were outliers and were, hence, discarded in the analysis. Ultimately, we generated four spreadsheets with the monthly climatic and topographic information jointly with corresponding monthly soil moisture contents and remotely sensed autumn grass senescence values. The four monthly spreadsheets were further split into eight spreadsheets based on the vegetation index (i.e., the NDRE or the Chlred-edge) as the predictor variable. The data were separately split into 80 and 20 for calibration and validation, respectively, and imported into R version 4.1.3 ([25] R Core Team) for further analysis (R Core Team, Vienna, Austria). Four popular regression algorithms (i.e., the PLSR, MLR, RFR, and CART) were employed in each monthly NDRE and Chlred-edge spreadsheet to test the association between the remotely sensed autumn grass senescence and the climatic factors and topography. A 10-fold-cross validation approach was used at each stage of analysis to evaluate the model performances based on the obtainable Root-Mean-Square Error (RMSE), the coefficient of determination (R^2), and the Mean Absolute Error (MAE).

2.6. Model Optimization and Identification of Key Environmental Determinants of Autumn Grassland Senescence

According to the performance of the four popular algorithms employed in Section 2.5, one superior model was identified using the RMSE, R^2, and MAE. The model was identified by averaging all the RMSEs, MAEs, and R^2s obtained throughout the four months of investigation. The model that yielded the lowest MAE and RMSE jointly with the highest R^2 was determined to be the best and was, hence, selected for the final prediction of remotely sensed autumn grass senescence with climatic factors and topography. As the superior algorithm, the RFR was adopted and eight final models were built to individually relate the monthly remotely sensed autumn grass senescence values (i.e., NDRE and the Chlred-edge) with their respective monthly climatic and topographic factors. These final models were optimized by tuning their *ntree*, *mtry*, and *nodesize* values. *ntrees* ranged between 300 and 1200, *mtrys* was between 2 and 16, while *nodesizes* was set to 1 throughout the analysis. The final prediction results were judged based on the RMSEs and their R^2s. Next, we averaged all the monthly predictor (i.e., NDRE and the Chlred-edge) and response (i.e., climatic and topographic) variables. The outcome was a set of two spreadsheets, first with the NDRE and second with the Chlred-edge as predictors, along with their monthly averages of topographic and climatic factors. Pearson's product-moment correlation tests were conducted in each set of the spreadsheet to determine the sensitivity of each climatic and topographic factor to the remotely sensed autumn grass senescence. The significance of each topographic or climatic variable in influencing the occurrence of autumn grassland senescence was judged by the *p*-value ($p \leq 0.05$).

3. Results

3.1. Descriptive Statistics

Table 2 provides the descriptive statistics of the remotely sensed autumn grass senescence plus climatic and topographic factors used in this study. Overall, the estimates of autumn grassland senescence based on the NDRE increased with a decrease in the Chlred-edge across the four-month period. In addition, there were no significant variations between the NDRE and the Chlred-edge values of autumn grass senescence from March to June. However, in March, the values of the $NDVI_{705}$-based autumn grass senescence were higher than those of the CHL-RED-EDGE-derived autumn grassland senescence. In addition, monthly means of all the topographic factors (i.e., aspect, elevation, and slope) did not show differences across the four-month period, while monthly means of the climatic variables (i.e., T_{min} and T_{max}, soil moisture, rainfall, and solar radiation) showed notable variations. Specifically, the means of the solar radiation, T_{min} and T_{max}, demonstrated consistent declines throughout the four months, whereas the observable decreases in rainfall and soil moisture from March to May were followed by an increase in June (Table 2).

Table 2. Descriptive statistics of the data gathered and retrieved for analysis.

Month	Variable	Min	Max	Mean	Stdv
March	NDRE	0.248	0.532	0.396	0.057
	Chlred-edge	0.239	0.519	0.357	0.058
	Aspect	7.723	340.649	144.777	87.127
	Elevation	1273	1412	1340	30.359
	Slope	0.512	19.411	5.702	3.860
	T_{max}	25.5	25.85	25.65	0.131
	T_{min}	13.68	14.66	14.13	0.398
	Radiation	22,878	232,161	150,843	65,496.12
	Rainfall	69.44	87.65	79.39	7.095
	Soil moisture	12.5	34.9	22.43	3.764
April	NDRE	0.182	0.477	0.346	0.051
	Chlred-edge	0.266	0.562	0.390	0.056
	Aspect	7.723	340.649	144.777	87.127
	Elevation	1273	1412	1340	30.359
	Slope	0.512	19.411	5.702	3.860
	T_{max}	24.51	25.08	24.78	0.217
	T_{min}	11.25	12.21	11.71	0.387
	Radiation	20,736	256,029	138,918	75,657.96
	Rainfall	58.5	64.74	62.04	2.137
	Soil moisture	10.1	30.1	16.36	4.505
May	NDRE	0.108	0.291	0.223	0.034
	Chlred-edge	0.266	0.562	0.390	0.049
	Aspect	7.723	340.649	144.777	87.127
	Elevation	1273	1412	1340	30.359
	Slope	0.512	19.411	5.702	3.860
	T_{max}	22.2	22.85	22.51	0.262
	T_{min}	8.481	9.672	9.057	0.488
	Radiation	19,653	304,608	137,763	87,583.85
	Rainfall	13.86	15.25	14.64	0.401
	Soil moisture	0.685	21.030	11.269	4.289
June	NDRE	−0.004	0.203	0.113	0.050
	Chlred-edge	0.522	1.076	0.666	0.111
	Aspect	7.723	340.649	144.777	87.127
	Elevation	1273	1412	1340	30.359
	Slope	0.512	19.411	5.702	3.860
	T_{max}	20.43	21.14	20.77	0.283
	T_{min}	6.876	7.919	7.379	0.418
	Radiation	22,430	303,014	131,301	89,098.69
	Rainfall	30.46	37.7	34.34	2.862
	Soil moisture	10.8	26.7	18.97	3.898

3.2. Remotely Sensed Autumn Grass Senescence with Climatic and Topographic Variables

Based on the results from the preliminary analysis (Table 3), the prediction outputs of the four popular regression models (i.e., the PLSR, MLR, CART, and the RFR) adopted in the study were generally significant. Specifically, the RFR outperformed all the other algorithms when using both the NDRE and the Chlred-edge as predictors throughout the four months considered in this investigation. This was demonstrated by the low RMSE and MAE with high R^2. These results (Table 3) further indicated that the CART was the second most important algorithm in the four months of analysis. On the other hand, the performance of the PSLR was generally inferior throughout the various stages of the analysis.

Table 3. Performance of the adopted algorithms based on the R^2, MEA, and the RMSE.

Month	Predictor Variable	Algorithm	RMSE	R^2	MAE
March	NDRE	PLS	0.046	0.39	0.037
		CART	0.042	0.47	0.033
		MLR	0.041	0.46	0.032
		RFR	0.039	0.50	0.031
	Chlred-edge	PLS	0.053	0.38	0.042
		CART	0.045	0.45	0.037
		MLR	0.046	0.46	0.036
		RFR	0.044	0.50	0.035
April	NDRE	PLS	0.038	0.35	0.031
		CART	0.034	0.63	0.028
		MLR	0.038	0.50	0.030
		RFR	0.035	0.62	0.026
	Chlred-edge	PLS	0.042	0.34	0.034
		CART	0.041	0.42	0.031
		MLR	0.043	0.42	0.034
		RFR	0.041	0.55	0.032
May	NDRE	PLS	0.024	0.52	0.020
		CART	0.024	0.50	0.018
		MLR	0.026	0.49	0.021
		RFR	0.022	0.53	0.017
	Chlred-edge	PLS	0.043	0.30	0.033
		CART	0.036	0.46	0.029
		MLR	0.043	0.36	0.036
		RFR	0.036	0.56	0.028
June	NDRE	PLS	0.041	0.36	0.033
		CART	0.046	0.42	0.035
		MLR	0.041	0.47	0.034
		RFR	0.033	0.68	0.026
	Chlred-edge	PLS	0.091	0.35	0.077
		CART	0.082	0.53	0.060
		MLR	0.101	0.33	0.078
		RFR	0.081	0.60	0.058

Moreover, the averaged prediction outputs of the adopted algorithms across the four-month period of the investigation maintained the findings presented in Table 3 that the RFR was the most useful model in associating the remotely sensed autumn grass senescence with climatic and topographic factors (Figure 2). A closer look at Figure 2a–c indicates that the RFR is the only algorithm that had a low RMSE and MAE with a high R^2 followed by CART. On the contrary, the PLSR displayed inferior performance based on two of the three model evaluation matrices (i.e., the R^2 and the MAE).

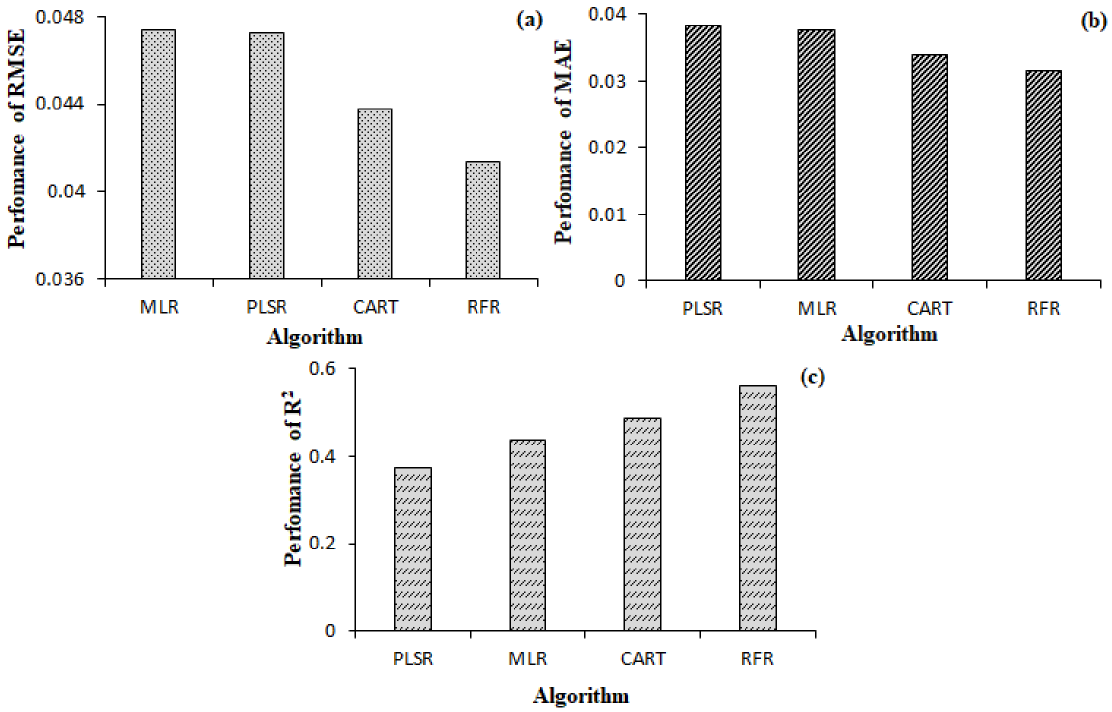

Figure 2. Algorithms' performances based on the (**a**) RMSE, (**b**) MAE, and the (**c**) R^2.

The final RFR models showed an improved explanation of the association between the remotely sensed autumn grass senescence and topographic and climatic factors when using both predictors across the four months considered (Table 4). For instance, when using the NDRE and the climatic and topographic factors in March, the model yielded an RMSE of 0.017 and an R^2 of 0.69 while obtaining an RMSE and an R^2 of 0.023 and 0.59, respectively, when using the Chlred-edge. Likewise, the NDRE recorded an RMSE of 0.012 and an R^2 of 0.71 in April, whereas the Chlred-edge produced an RMSE of 0.018 and R^2 of 0.60. Similarly, both the NDRE and the Chlred-edge reported RMSEs and R^2s of 0.056 and 0.014, as well as 0.56 and 0.69 in May, respectively. Moreover, the NDRE showed an RMSE and R^2 of 0.013 and 0.71, while the Chlred-edge obtained an RMSE of 0.056 and R^2 of 0.72 in June, respectively. Important variables for the final prediction models are presented in Figure 3. The predictive performance of each variable was assessed based on the obtainable Out of Bag error rate, which increases with significance.

Table 4. Optimal RFR results for the relationships between remotely sensed grass senescence and climatic factors and topography.

	NDRE		Chlred-Edge	
Month	**RMSE**	**R^2**	**RMSE**	**R^2**
March	0.017	0.69	0.023	0.59
April	0.012	0.71	0.018	0.60
May	0.056	0.56	0.014	0.69
June	0.013	0.71	0.056	0.72

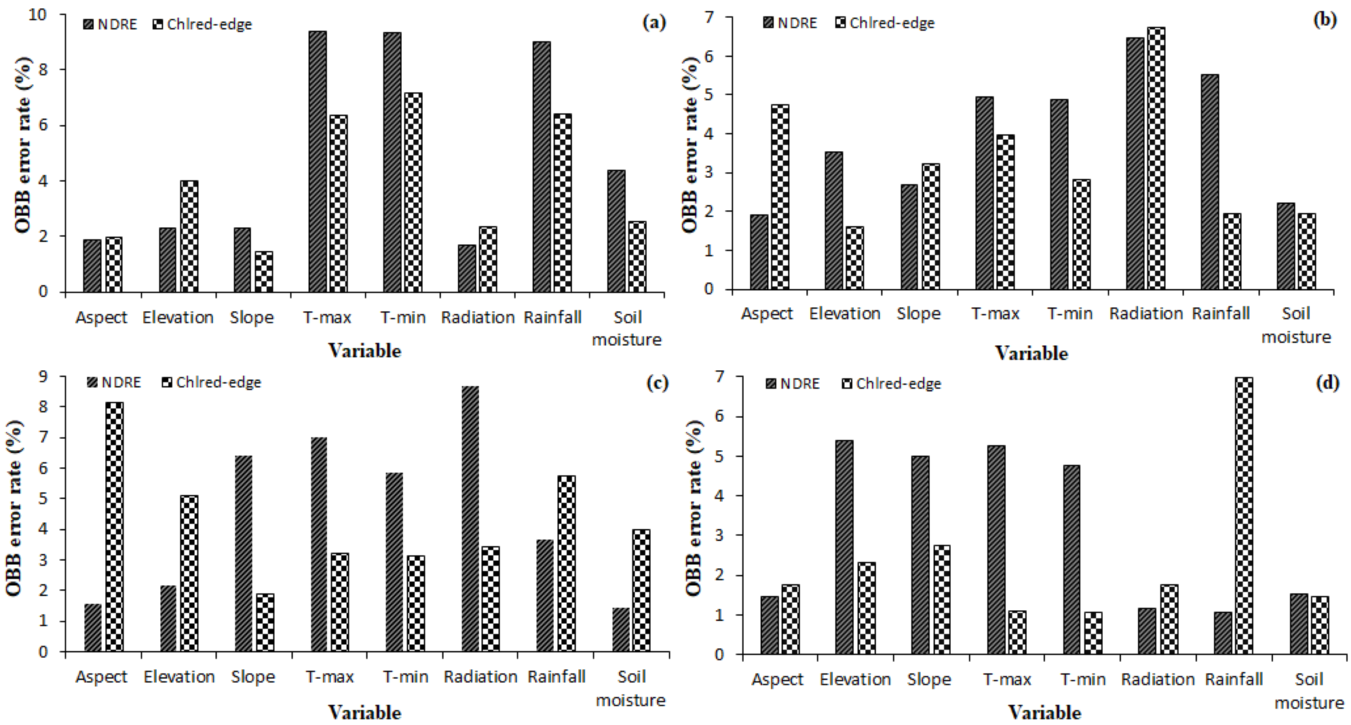

Figure 3. RFR model's variable importance for assessing the response of remotely sensed autumn grass senescence against the climatic and topographic factors in (**a**) March, (**b**) April, (**c**) May, and (**d**) June.

3.3. Climatic and Topographic Drivers of the Autumn Grassland Senescence

Using the monthly averages of the predictors (i.e., the NDRE and the Chlred-edge) against the response variables (i.e., topographic and climatic variables), we identified the key drivers influencing the occurrence of autumn grassland senescence (Table 5). In general, our findings showed that only the climatic factors were sensitive to the occurrence of autumn grassland senescence. Specifically, the T_{min} and T_{max}, jointly with soil moisture, were identified as the most influential factors in the occurrence of autumn grass senescence, as shown by their significance levels ($p \leq 0.05$). Obtainable R^2 values for the three climatic factors that significantly influence the occurrence of autumn grass senescence were 1.00, 0.98, and 0.81 based on the NDRE and −1.00, −0.96, and −0.78 when using the Chlred-edge, respectively. Conversely, even though they displayed good R^2 values (i.e., between 0.76 and 0.93), the insignificant *p*-values ($p \geq 0.05$) highlighted the poor contribution of these other climatic variables in explaining the occurrence of autumn grass senescence in the study area. With regard to the topographic factors, only the slope showed good R^2 values (i.e., −0.80 and 0.75 when using the NDRE and the Chlred-edge, respectively); otherwise, they were all insignificant when considering the *p*-values ($p \geq 0.05$). Table 5 shows the contribution of environmental factors on autumn grassland senescence, with significant variables in bold.

The sensitivity of the topographic and climatic factors in influencing the occurrence of autumn grass senescence in the study area was further emphasized by the value of the *t*-statistics, with higher values signifying the importance and vice versa.

Table 5. Correlations between remotely sensed grass senescence and climatic factors and topography. Influential variables are shown in bold.

Variable	NDRE			Chlred-Edge		
	t-Statistics	*p*-Value	R^2	*t*-Statistics	*p*-Value	R^2
Topographic factors						
Aspect	−0.597	0.611	−0.39	0.492	0.672	0.33
Elevation	0.163	0.886	0.11	−0.276	0.809	−0.19
Slope	−1.865	0.203	−0.80	1.588	0.253	0.75
Climatic factors						
T_{max}	55.095	**0.000**	1.00	−14.388	**0.005**	−1.00
T_{min}	6.832	**0.021**	0.98	−4.806	**0.041**	−0.96
Radiation	3.502	0.073	0.93	−2.852	0.104	−0.90
Rainfall	1.881	0.201	0.80	−1.661	0.239	−0.76
Soil moisture	6.579	**0.031**	0.81	−4.461	**0.040**	−0.78

Figure 4 shows the response of the remotely sensed autumn grass senescence (i.e., NDRE and Chlred-edge) to the most influential variables (i.e., T_{min}, T_{max}, and the soil moisture). Figure 4a–c illustrate the remotely sensed autumn grass senescence based on the NDRE, while Figure 4d–f display the remotely sensed autumn grass senescence based on the Chlred-edge. Overall, the effect of time lag was evident between the occurrence of autumn grassland senescence and the change in sensitive variables. The NDRE-based autumn grass senescence indicated a continuous decline with a decrease in both the T_{min} and T_{max} during the autumn season. On the other hand, a synonymous decline in the NDRE-based autumn grass senescence with soil moisture was followed by a sudden increase in soil moisture in June. Figure 4d–f indicate an inverse relationship between the Chlred-edge-based autumn grass senescence and the influential variables. Generally, the consistent drop in T_{min}, T_{max}, and the soil moisture values was concurrent with the increasing Chlred-edge-based autumn grass senescence estimates.

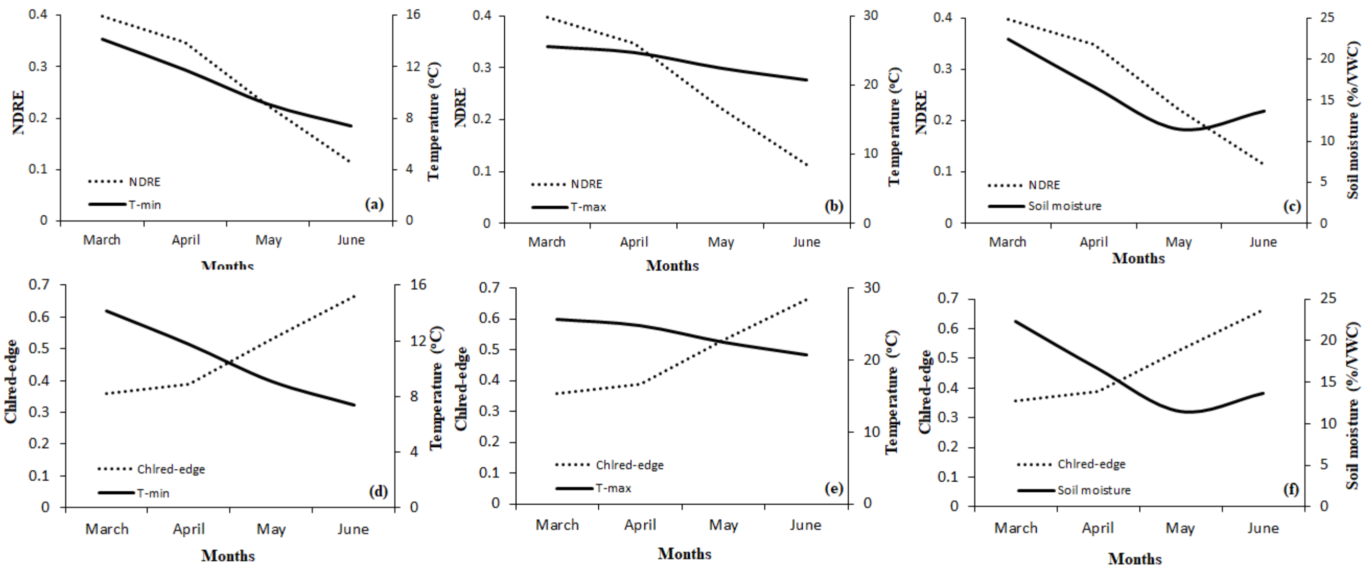

Figure 4. The responses of the (**a**–**c**) NDRE-based autumn grass senescence to (**a**) T_{min}, (**b**) T_{max}, and (**c**) soil moisture together with those of the (**d**–**f**) Chlred-edge-based autumn grass senescence to (**d**) T_{min}, (**e**) T_{max}, and (**f**) soil moisture through time.

4. Discussion

The present study has shown the value of the multi-temporal remotely acquired Sentinel 2 satellite data in elucidating the occurrence of autumn senescence along climatic and topographic gradients in the subtropical sour-veld grassland ecosystems. This has been a limitation in understanding the dynamics around the occurrence of autumn senescence as well as the subsequent impact on foraging resource productivity and feed availability in these regions. Our findings indicated that the occurrence of autumn grassland senescence in the present study site is controlled by climatic drivers, particularly the soil moisture, T_{min}, and T_{max} rather than topographic factors ($p \leq 0.05$ in Table 5). Although not pronounced in the current findings, the sensitivity of air temperature variables (i.e., T_{max} and T_{min}) in influencing the occurrence of autumn grassland senescence in the area could be attributed to the reported extremities of these variables [26]. For instance, the observed consistent decline in air temperatures (Table 2) is believed to have promoted irregular frost events, as they are known to be a common phenomenon in the area during this period [27] and, hence, grass senescence. These results concur with studies indicating that extreme-temperature conditions affect the natural processes of photosynthetic enzymes and thereby accelerate or delay chlorophyll deterioration [4,6,28], whereas water shortages are known to influence plant carboxylation reaction, hence fast-tracking chlorophyll degradation and plant senescence [1,5,12,29].

Conversely, although solar radiation and rainfall are known to be key climatic factors influencing plant phenology [2], their impact was not significant (Table 5). However, these results should be discussed with caution, as the observed poor relationship between the remotely sensed autumn grass senescence and rainfall and solar radiation may not be universally constant, i.e., could be site-specific as a result of topographic and micro-climatic conditions. Specifically, the recorded poor correlation between autumn grassland senescence and rainfall in this study may possibly be a consequence of the high variability in rainfall during the same period [26], which could destruct the uniformity in the phenology of the grass. Similarly, the poor relationship notable between the autumn grass senescence and solar radiation could be justified by the relatively uniform topography of the study area, which was observed during field data collection. Meanwhile, our assumption is that meaningful characterization of the links between the remotely sensed autumn grass senescence and the incoming solar radiation and topographic factors such as slope, aspect, and elevation requires heterogeneity in the landscape, which is possible in pronounced mountainous and valley areas [2], also indicated that heterogeneity in topography promotes spatial distinction in vegetation phenology regardless of the similarity in the age of the floral species. Our results further showed the effect of the time lag between the occurrence of autumn grass senescence and the change in sensitive climatic factors (Figure 4), thereby suggesting that the chlorophyll breakdown is not concurrent with, but follows the triggering effect of, the environmental cue. Evidently, the significance of understanding the response of autumn grassland senescence to changes in climatic and topographic factors cannot be over-emphasized, particularly in countries such as South Africa, considering the projected shifts in seasonal patterns [30], which may further alter the current dynamics in phenological stages such as the autumn grassland senescence, leading to potential forage deficiencies, especially during dry seasons. With its ability to either shorten or extend the growing season of the floral species, and hence productivity [8], the understanding of the links between autumn grass senescence and environmental factors may help to strengthen our projections on the possible timing and duration of the autumn grassland senescence, which will, in turn, improve our assessment of fodder bank capacities for quality forage provision. Whereas this highlights the essence of future research on this subject matter, the emphasis of such work should be on multi-year studies conducted on heterogeneous terrains, while fully embracing the potential impact of frost activities in the analysis.

With regard to the performance of the RFR model, our results reinforce the evidence presented in previous studies that this model is robust when explaining ecological problems based on remotely acquired datasets [15,31]. Again, although the findings in Figure 3 may give an impression that the topographic factors were among the important variables in April, May, and June, a correct view is that these variables were only important in displaying the monthly relationship with the tested variables, which does not necessarily reflect the autumn grassland senescence in our case. According to our approach in this study, the autumn grassland senescence was explained based on the averaged performance of the month-to-month contributions of each variable, and the variables that were consistently significant were identified as the environmental drivers of autumn grassland senescence.

5. Conclusions

The present study examined the relationship between remotely sensed autumn grass senescence and the climatic factors and topography in the subtropical sour-veld grasslands of the Midlands region, KwaZulu-Natal, South Africa. The study employed the Sentinel 2 derivatives using the PLSR, MLR, CART, and RFR models, and the RFR model emerged as the superior model. Among the best of the model outputs, RMSEs of 0.017, 0.012, 0.056, and 0.013 as well as R^2s of 0.69, 0.71, 0.56, and 0.71 for the NDRE, with RMSEs and R^2s of 0.023, 0.018, 0.014, and 0.056 as well as 0.59, 0.60, 0.69, and 0.72 for the Chlred-edge in March, April, May, and June, respectively, were obtained. The results further showed that T_{min}, T_{max}, and soil moisture were the most influential factors in the occurrence of autumn grassland senescence at the study site. However, the observable poor relationship between autumn grass senescence and the other climatic factors and topography is believed to be indicative of the micro-climatic conditions and the relative homogeneity in the topography. However, given that the study was carried over a season, it does not reflect the possible year-to-year climatic changes and, hence, cannot be used to draw finality on the relationship between the tested variables. Therefore, for a conclusive understanding of the overlaps between autumn grass senescence and climatic and topographic factors, we suggest further investigation, particularly focusing on multi-year studies conducted in heterogeneous landscapes and taking into account the effect of frost occurrences in the analysis.

Author Contributions: Conceptualization, L.R., O.M. and R.S.; methodology, L.R. and O.M.; software, L.R.; validation, O.M. and J.O.; formal analysis, L.R.; investigation, L.R.; resources, L.R. and O.M.; data curation, L.R.; writing—original draft preparation, L.R.; writing—review and editing, J.O. and O.M.; visualization, L.R.; supervision, O.M. and J.O.; project administration, L.R. and O.M.; funding acquisition, O.M. and R.S. All authors have read and agreed to the published version of the manuscript.

Funding: This study was funded by the National Research Foundation (NRF) of South Africa, Research Chair initiative in Land Use Planning and Management (Grant Numbers: 84157).

Data Availability Statement: The data could not be made available at the present moment because the study is part of an ongoing bigger project and publishing its data at this stage may compromise the scope of the subsequent chapters.

Acknowledgments: The authors would like the thank the South African Weather Services (SAWS) for providing rainfall and temperature data. In addition, recognition is given to Mthembeni Mngadi, Omosalewa Odebiri, Asekho Mantintsilili, Nkululeko Dladla, and Lesogo Hlwayi for their field data collection assistance. In addition, the authors express their words of thanks to Andile Etah Mshengu for her kind support with the processing of finances and booking of vehicles for site visits.

Conflicts of Interest: The authors declare no conflict of interest.

References

1. Tao, Z.; Ge, Q.; Wang, H.; Dai, J. The important role of soil moisture in controlling autumn phenology of herbaceous plants in the Inner Mongolian steppe. *Land Degrad. Dev.* **2021**, *32*, 3698–3710. [CrossRef]
2. Shoko, C.; Mutanga, O.; Dube, T. Remotely sensed C3 and C4 grass species aboveground biomass variability in response to seasonal climate and topography. *Afr. J. Ecol.* **2019**, *57*, 477–489. [CrossRef]
3. Wu, C.; Wang, X.; Wang, H.; Ciais, P.; Peñuelas, J.; Myneni, R.B.; Desai, A.R.; Gough, C.M.; Gonsamo, A.; Black, A.T. Contrasting responses of autumn-leaf senescence to daytime and night-time warming. *Nat. Clim. Change* **2018**, *8*, 1092–1096. [CrossRef]

4. Liu, G.; Chen, X.; Zhang, Q.; Lang, W.; Delpierre, N. Antagonistic effects of growing season and autumn temperatures on the timing of leaf coloration in winter deciduous trees. *Glob. Change Biol.* **2018**, *24*, 3537–3545. [CrossRef] [PubMed]
5. Tao, Z.; Wang, H.; Dai, J.; Alatalo, J.; Ge, Q. Modeling spatiotemporal variations in leaf coloring date of three tree species across China. *Agric. For. Meteorol.* **2018**, *249*, 310–318. [CrossRef]
6. Liu, Q.; Fu, Y.H.; Zeng, Z.; Huang, M.; Li, X.; Piao, S. Temperature, precipitation, and insolation effects on autumn vegetation phenology in temperate China. *Glob. Change Biol.* **2016**, *22*, 644–655. [CrossRef] [PubMed]
7. McKean, J.; Buechel, S.; Gaydos, L. Remote sensing and landslide hazard assessment. *Photogramm. Eng. Remote Sens.* **1991**, *57*, 1185–1193.
8. Gepstein, S.; Sabehi, G.; Carp, M.J.; Hajouj, T.; Nesher, M.F.O.; Yariv, I.; Dor, C.; Bassani, M. Large-scale identification of leaf senescence-associated genes. *Plant J.* **2003**, *36*, 629–642. [CrossRef]
9. Royimani, L.; Mutanga, O.; Dube, T. Progress in remote sensing of plant senescence: A review on the challenges and opportunities. *IEEE J. Sel. Top. Appl. Earth Obs. Remote Sens.* **2021**, *14*, 7714–7723. [CrossRef]
10. Royimani, L.; Mutanga, O.; Odindi, J.; Sibanda, M.; Chamane, S. Determining the onset of autumn grass senescence in subtropical sour-veld grasslands using remote sensing proxies and the breakpoint approach. *Ecol. Inform.* **2022**, *69*, 101651. [CrossRef]
11. Anderegg, J.; Yu, K.; Aasen, H.; Walter, A.; Liebisch, F.; Hund, A. Spectral vegetation indices to track senescence dynamics in diverse wheat germplasm. *Front. Plant Sci.* **2020**, *10*, 1749. [CrossRef] [PubMed]
12. Munné-Bosch, S.; Alegre, L. Die and let live: Leaf senescence contributes to plant survival under drought stress. *Funct. Plant Biol.* **2004**, *31*, 203–216. [CrossRef] [PubMed]
13. Mariën, B.; Dox, I.; De Boeck, H.J.; Willems, P.; Leys, S.; Papadimitriou, D.; Campioli, M. Does drought advance the onset of autumn leaf senescence in temperate deciduous forest trees? *Biogeosciences* **2021**, *18*, 3309–3330. [CrossRef]
14. Royimani, L.; Mutanga, O.; Odindi, J.; Dube, T.; Matongera, T.N. Advancements in satellite remote sensing for mapping and monitoring of alien invasive plant species (AIPs). *Phys. Chem. Earth Parts A/B/C* **2019**, *112*, 237–245. [CrossRef]
15. Royimani, L.; Mutanga, O.; Odindi, J.; Zolo, K.S.; Sibanda, M.; Dube, T. Distribution of *Parthenium hysterophoru* L. with variation in rainfall using multi-year SPOT data and random forest classification. *Remote Sens. Appl. Soc. Environ.* **2019**, *13*, 215–223. [CrossRef]
16. Sibanda, M.; Mutanga, O.; Rouget, M. Comparing the spectral settings of the new generation broad and narrow band sensors in estimating biomass of native grasses grown under different management practices. *GISci. Remote Sens.* **2016**, *53*, 614–633. [CrossRef]
17. Makanza, R.; Zaman-Allah, M.; Cairns, J.E.; Magorokosho, C.; Tarekegne, A.; Olsen, M.; Prasanna, B.M. High-throughput phenotyping of canopy cover and senescence in maize field trials using aerial digital canopy imaging. *Remote Sens.* **2018**, *10*, 330. [CrossRef]
18. Renier, C.; Waldner, F.; Jacques, D.C.; Ebbe, M.A.B.; Cressman, K.; Defourny, P. A dynamic vegetation senescence indicator for near-real-time desert locust habitat monitoring with MODIS. *Remote Sens.* **2015**, *7*, 7545–7570. [CrossRef]
19. Sibanda, M.; Onisimo, M.; Dube, T.; Mabhaudhi, T. Quantitative assessment of grassland foliar moisture parameters as an inference on rangeland condition in the mesic rangelands of southern Africa. *Int. J. Remote Sens.* **2021**, *42*, 1474–1491. [CrossRef]
20. Singh, L.; Mutanga, O.; Mafongoya, P.; Peerbhay, K.Y. Multispectral mapping of key grassland nutrients in KwaZulu-Natal, South Africa. *J. Spat. Sci.* **2018**, *63*, 155–172. [CrossRef]
21. Delta-T Devices. Thetakit User Guide: ML3-Kit. Available online: https://delta-t.co.uk/wp-content/uploads/2016/09/ML3_Kit_User_Guide_ver_1.0.pdf (accessed on 22 February 2021).
22. Dube, T.; Mutanga, O. The impact of integrating WorldView-2 sensor and environmental variables in estimating plantation forest species aboveground biomass and carbon stocks in uMgeni Catchment, South Africa. *ISPRS J. Photogramm. Remote Sens.* **2016**, *119*, 415–425. [CrossRef]
23. Ruiz-Arias, J.; Tovar-Pescador, J.; Pozo-Vázquez, D.; Alsamamra, H. A comparative analysis of DEM-based models to estimate the solar radiation in mountainous terrain. *Int. J. Geogr. Inf. Sci.* **2009**, *23*, 1049–1076. [CrossRef]
24. Kumar, L.; Skidmore, A.K.; Knowles, E. Modelling topographic variation in solar radiation in a GIS environment. *Int. J. Geogr. Inf. Sci.* **1997**, *11*, 475–497. [CrossRef]
25. R Core Team. *R: A Language and Environment for Statistical Computing*; R Foundation for Statistical Computing: Vienna, Austria, 2021; Available online: https://www.R-project.org/ (accessed on 5 April 2022).
26. Ndlovu, M.; Clulow, A.D.; Savage, M.J.; Nhamo, L.; Magidi, J.; Mabhaudhi, T. An assessment of the impacts of climate variability and change in KwaZulu-Natal Province, South Africa. *Atmosphere* **2021**, *12*, 427. [CrossRef]
27. Ismail, R.; Crous, J.; Sale, G.; Morris, A.R.; Peerbhay, K.Y. Developing a satellite-based frost risk model for the Southern African commercial forestry landscape. *South. For. A J. For. Sci.* **2021**, *83*, 10–18. [CrossRef]
28. Fracheboud, Y.; Luquez, V.; Bjorken, L.; Sjodin, A.; Tuominen, H.; Jansson, S. The control of autumn senescence in European aspen. *Plant Physiol.* **2009**, *149*, 1982–1991. [CrossRef]

29. Sade, N.; del Mar Rubio-Wilhelmi, M.; Umnajkitikorn, K.; Blumwald, E. Stress-induced senescence and plant tolerance to abiotic stress. *J. Exp. Bot.* **2018**, *69*, 845–853. [CrossRef]
30. Van der Walt, A.J.; Fitchett, J.M. Statistical classification of South African seasonal divisions on the basis of daily temperature data. *S. Afr. J. Sci.* **2020**, *116*, 1–15. [CrossRef]
31. Mutanga, O.; Adam, E.; Cho, M.A. High density biomass estimation for wetland vegetation using WorldView-2 imagery and random forest regression algorithm. *Int. J. Appl. Earth Obs. Geoinf.* **2012**, *18*, 399–406. [CrossRef]